Self-Assembly and Transport Limitations in Confined Nafion Films

ARTICLE *in* MACROMOLECULES · FEBRUARY 2013

Impact Factor: 5.8 · DOI: 10.1021/ma301999a

9 AUTHORS, INCLUDING:

Miguel A Modestino
École Polytechnique Fédérale de Lausanne
25 PUBLICATIONS **334** CITATIONS
SEE PROFILE

Devproshad K. Paul
The University of Calgary
23 PUBLICATIONS **370** CITATIONS
SEE PROFILE

Shudipto Konika Dishari
Pennsylvania State University
9 PUBLICATIONS **113** CITATIONS
SEE PROFILE

Frances I Allen
University of California, Berkeley
27 PUBLICATIONS **207** CITATIONS
SEE PROFILE

Macromolecules

Article

pubs.acs.org/Macromolecules

Self-Assembly and Transport Limitations in Confined Nafion Films

Miguel A. Modestino,*[,†] Devproshad K. Paul,[‡] Shudipto Dishari,[§] Stephanie A. Petrina,[§] Frances I. Allen,[∥] Michael A. Hickner,[§] Kunal Karan,[‡,#] Rachel A. Segalman,[†] and Adam Z. Weber[⊥]

[†]Department of Chemical and Biomolecular Engineering, University of California, Berkeley, California 94720, United States, and Materials Science Division, Lawrence Berkeley National Laboratory, Berkeley, California 94720, United States

[‡]Department of Chemical Engineering, Queen's University, Kingston, Ontario K7L 3N6, Canada

[§]Department of Materials Science and Engineering, The Pennsylvania State University, University Park, Pennsylvania 16802, United States

[∥]National Center for Electron Microscopy, Lawrence Berkeley National Laboratory, and Department of Materials Science and Engineering, University of California, Berkeley, California 94720, United States

[⊥]Environmental Energy Technologies Division, Lawrence Berkeley National Laboratory, Berkeley, California 94720, United States

Supporting Information

ABSTRACT: Ion-conducting polymers are important materials for a variety of electrochemical applications. Perfluorinated ionomers, such as Nafion, are the benchmark materials for proton conduction and are widely used in fuel cells and other electrochemical devices including solar-fuel generators, chlor-alkali cells, and redox flow batteries. While the behavior of Nafion in bulk membranes (10 to 100s μm thick) has been studied extensively, understanding its properties under thin-film confinement is limited. Elucidating the behavior of thin Nafion films is particularly important for the optimization of fuel-cell catalyst layers or vapor-operated solar-fuel generators, where a thin film of ionomer is responsible for the transport of ions to and from the active electrocatalytic centers. Using a combination of transport-property measurements and structural characterization, this work demonstrates that confinement of Nafion in thin films induced thickness-dependent proton conductivity and ionic-domain structure. Confining Nafion films to thicknesses below 50 nm on a silicon substrate results in a loss of microphase separation of the hydrophilic and hydrophobic domains, which drastically increases the material's water uptake while in turn decreasing its ionic conductivity.

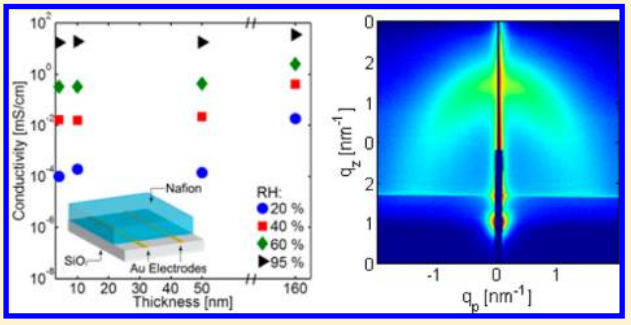

INTRODUCTION

Research in energy generation, conversion, and storage has dramatically increased due to the need for a sustainable energy infrastructure. Technologies including fuel cells, redox flow batteries, and solar-fuel generators represent promising options as their combination can result in clean and sustainable stationary and transportation energy solutions. These electrochemical devices involve multiple functional layers with varying physics (ion conduction, multiphase flow, etc.), combinations of materials, and generally require the transport of charged intermediates (i.e., protons or anions) through a solid-state polyelectrolyte into inorganic catalytic inclusions where redox reactions occur.[1−4] Transport across these hybrid polymer/inorganic interfaces is crucial for the operation of the devices, in particular in fuel-cell catalysts layers or vapor-fed solar-fuel devices,[5,6] where ion conduction occurs through\along ionomer thin films covering the catalytic centers.[7−9] The structure of polyelectrolytes when confined to a thin film can be affected significantly, and its transport characteristics can drastically differ from the behavior in bulk membranes.[10,11]

Perfluorinated sulfonic acid (PFSA) ionomers, such as Nafion, are the most widely used materials for electrochemical applications requiring proton conduction. Nafion's structure is comprised of a perfluorinated backbone that provides both mechanical and chemical stability and randomly placed tethered side chains terminated with sulfonic acid groups which impart its remarkable proton-conduction capabilities.[12] Its structure in bulk membranes (10 to 100s μm thick) has been extensively studied using both small- and wide-angle X-ray and neutron scattering techniques. Typical scattering profiles of Nafion demonstrate a phase-separated morphology, which is comprised of periodic ionic domains with a scattering maximum at q = 1−2 nm^{-1} (referred to as ionomer peak), and a semicrystalline matrix contributing to a broad scattering peak at lower q-values (0.4−0.5 nm^{-1}) arising from intercrystallite spacing.[13−19] The structure in these membranes is predom-

Received: September 21, 2012
Revised: January 11, 2013
Published: January 23, 2013

inantly dominated by the bulk material, as the near-interface regions do not account for a significant volume fraction of the system. Furthermore, Nafion's ionic domains can absorb up to 15 or 22 water molecules per sulfonic acid group when equilibrated in saturated vapor or liquid water, respectively,[20−24] and the ionic conductivity of the material is significantly affected by its water content.[25,26] Although the structure and transport characteristics of Nafion membranes have been described in depth in the literature, the behavior of this material when confined to a thin-film morphology is still not well understood.

Thin-film confinement is known to affect the phase behavior of uncharged block copolymer systems.[27−32] In thin films, surface interactions and confinement to thicknesses that approach the characteristic domain size of the copolymers can cause anisotropy in the orientation of domains and pose significant limitations for self-assembly, resulting in morphologies that differ from the bulk. Ionomers are more complex than many well-studied polymers due to the presence of electrostatic interactions, hydrogen bonding, and less well-defined chain structure, but their self-assembly is also expected to be affected by wetting interactions at both the substrate and free (vapor) interfaces as well as by topological confinement effects. Recent studies have demonstrated that thin-film confinement as well as variations in substrate wetting interactions result in differences in orientations of ionic domains that limit water uptake.[33,34] Also, interactions at the top interface of films can result in different ionomer wetting in the presence of saturated vapor or liquid water.[18,35,36] All these morphological effects can help explain the observed limitations in water mobility[37] as well as ionic conductivity[38,39] when Nafion is topologically confined.

This work systematically analyzes the effect of thin-film confinement on proton conductivity and water uptake and provides insights into the morphological characteristics responsible for the transport limitations in thin films. Grazing incidence small-angle X-ray scattering (GISAXS) and transmission electron microscopy (TEM) are used to elucidate the structure of thin films and aid in the understanding of differences in water uptake and ionic transport under confinement.

EXPERIMENTAL SECTION

Materials. In the present study, three different types of SiO_2 substrates were employed. For ellipsometry and GISAXS measurements, silicon wafers with a 300 nm thermally grown SiO_2 layer were used. SiO_2-coated gold-electrode 6 MHz quartz crystals (Tangidyne, Greenville, SC) were employed as QCM substrates. For impedance measurements, thermally grown SiO_2 (2000 nm) supporting comb-shaped interdigitated array (IDA) of gold electrodes were used (110 gold teeth of 1 cm length, 10 μm in width and 50 nm thickness, separated 100 μm apart, Figure 1). Nafion (EW 1100) solution (5 wt %) in water−alcohol mixture (75/20 w/w alcohol to water) obtained from Ion Power was used as the stock Nafion solution. This stock solution was diluted to desired concentrations of 0.1, 0.25, 1, and 3 wt % by addition of isopropyl alcohol (IPA) (Sigma-Aldrich). The diluted solutions were sonicated for 5 min and equilibrated for at least 24 h. Nafion concentrations were chosen based on the findings of Paul et al.,[40] who determined that the corresponding thickness of self-assembled films to be about 4, 10, 55, and 160 nm, respectively.

Thin Film Preparation. Self-assembled thin films of Nafion were fabricated following the procedure developed by Karan and co-workers.[11,40] The substrates were subjected to several cleaning steps prior to film deposition (see Supporting Information). For fabrication of Nafion thin films, the substrates (bare SiO_2 and IDAs) were immersed in diluted Nafion solution for 12 h to allow for self-assembly. Subsequently, after carefully removing the substrate from the solution it was dried under flowing dry air. For preparation of Nafion films for QCM, the crystal was placed into the QCM holder with the SiO_2 coating side exposed. The loaded QCM holder was immersed in the required Nafion solution and dried as described above.

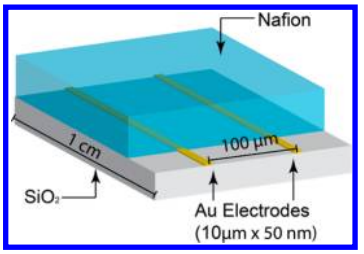

Figure 1. Schematic representation of thin film assembly used to measure in-plane ionic conductivity.

Thin-Film Conductivity Measurements. For conductivity determination, impedance spectroscopy measurements were accomplished by a two microprobe setup connected with a Solartron 1260 frequency-response analyzer coupled to a Solartron 1296 dielectric interface. The IDAs with Nafion films (Figure 1) were placed in an environmental chamber (Model 3911, Thermo Forma) with relative humidity (RH) and temperature control. All measurements were carried out at 25 °C, comparable to the conditions used for measurements of water uptake by QCM and thickness change by ellipsometry. A humidity sensor (CMOSENS Tec., Switzerland) was placed close to the IDA sample to monitor the local RH and temperature. Single-frequency impedance measurements were carried out to monitor the sample equilibration. When the impedance value no longer varied, the film was deemed to be equilibrated at the set RH and temperature. At this stage, impedance data were collected by applying an alternating potential of amplitude 100 mV over a frequency ranging from 10 MHz to 0.01 Hz. Further, at each RH and temperature, at least triplicate impedance data were collected for a given sample to ensure reproducibility. Smart impedance measurement software (Solartron Analytical) was used for data collection, and *Z*-view impedance software (Version 3.0a, Scribner Associates Inc.) was adopted for equivalent-circuit design, model fitting, and data analysis. The film conductivity (κ_f) was calculated from the fitted resistance (R_f) obtained from impedance measurements using[11]

$$\kappa_f = \frac{1}{R_f}\frac{d}{l(N-1)t}$$

where d is the space between the IDA electrodes (100 μm), t is the thickness of the film, l is the length of the teeth (1 cm), and N is the number of electrodes (110).

Water-Uptake Measurements. Film thicknesses were measured in situ under varying relative humidity (RH) using a J.A. Woollam RC2-XI dual rotating compensator multichannel spectroscopic ellipsometer. The change in the wave amplitude (Ψ) and phase shift (Δ) was measured over a spectral range of 240−1700 nm (0.75−5.15 eV). Once Ψ and Δ were characterized as a function of photon energy, a Lorentz oscillator-based homogeneous single slab model with no roughness was used to derive the thickness and optical properties of the polymer films on optically characterized substrates. The change in thickness and complex refractive index were calculated for films exposed to 0, 25, 50, 75, and 90% RH in an in-house constructed environmental cell held at ambient temperature. The cell was made with nonpolarizing fused silica windows to maximize the amount of light transmitted. The % thickness change or % swelling (S) as a function of RH was calculated from the ellipsometric data by

$$S\ (\%) = 100\% \times \frac{t_{RH} - t_0}{t_0}$$

dx.doi.org/10.1021/ma301999a | Macromolecules 2013, 46, 867−873

where t_{RH} is the thickness at a given RH and t_0 is the thickness at 0% RH.

Water uptake was measured using a QCM (Maxtek/Inficon, East Syracuse, NY) and Sauerbrey analysis. The entire QCM holder was enclosed in a poly(ethyelene) in-house constructed humidity chamber maintained at ambient temperature. The hydration number, λ (moles of water per mole of sulfonic acid group), was calculated from the mass uptake of the samples

$$\lambda = \frac{m_{RH} - m_0}{M_{H_2O}} \frac{1000}{m_0 IEC}$$

where m_{RH} is the sample mass at a given RH, m_0 is the mass of the dry sample, M_{H_2O} is the molecular mass of water, and IEC is the ion-exchange capacity (0.909 mmol/g).

For humidification in both ellipsometry and QCM experiments, air at the dew point was produced using a sparging system. The humidified wet air was mixed with a stream of dry air, and the flow rates of the wet and dry streams were varied using electronic mass-flow controllers (Omega FMA5512, Omega Engineering, Inc., Stamford, CT) to achieve a specific relative humidity at ambient pressure. A RH probe (Omega HX15-W) was connected to the gas outlet from the ellipsometry or QCM in-house constructed humidity chambers for in-situ monitoring of the relative humidity of the sample environment.

Grazing-Incidence Small-Angle X-ray Scattering Measurements. GISAXS measurements were performed as described previously in the literature.[33] Thin-film samples were placed into an in-house built environmental chamber with X-ray transparent Kapton windows. The sample cell was equilibrated at 100% RH at room temperature (20 °C) in less than 3 min, and GISAXS patterns were collected as a function of time for 25 min. All X-ray scattering experiments were performed in beamline 7.3.3 of the Advanced Light Source (ALS) at Lawrence Berkeley National Laboratory (LBNL).[41] The X-ray energy used was 10 keV, with a monochromator energy resolution E/dE of 100, and the patterns shown were acquired with a 2D Dectris Pilatus 1 M CCD detector (172 μm × 172 μm pixel size). All the GISAXS patterns presented here were collected at an incidence angle of α_i = 0.20°, well above the critical angle for Nafion and just below that of Si in order to probe the entire film structure.

Transmission Electron Microscopy Measurements. Nafion thin films for investigation by TEM were prepared by either spin-casting from Nafion-IPA solutions onto silicon with native oxide substrates and then floating off small sections onto copper mesh grids (for 20−100 nm films) in water or by casting directly onto holey silicon nitride grids (for 10 nm films). In this way, stable free-standing films were obtained. The films were not stained.

The TEM data were recorded using a 200MC Zeiss Libra microscope operated at 200 kV, at the National Center for Electron Microscopy, LBNL. In addition to standard bright-field imaging, the energy filter of the microscope was used for energy-filtered TEM spectrum imaging (EFTEM SI). An EFTEM SI data set was acquired by selecting a narrow energy slit (e.g., 5 eV) and collecting a series of images at sequential electron energy-loss positions over a given spectral range. Since polymers exhibit a wide-array of valence-electron configurations, the plasmon peak in the low-electron energy-loss range (<50 eV) can be used as a fingerprint for different polymer types. Consequently, we applied the technique of low-loss EFTEM SI,[42] using a recently developed advanced acquisition scheme,[43] and processed the data sets by principal component analysis to extract chemical maps based on subtle spectral differences between the plasmon peaks of the phase-separated Nafion domains.

RESULTS

Conductivity. This study focuses on a series of films with thicknesses ranging from 4 to 160 nm. Within this film thickness range, confinement effects are expected to have a significant impact on the structure and properties of the ionomer, in particular as the film thickness approaches the size of the hydrated domains (3−6 nm) and the reported diameter (3−5 nm) of rodlike structures in solution.[14,44−46] Furthermore, the characteristics observed for films of less than 10 nm are relevant for understanding the transport in catalyst layers where the ionomer exists as very thin films.[7−9] Figure 2 presents the proton conductivity of the ionomer thin films as a function of film thickness for various RHs (see Supporting Information for table of values). The obtained results show a significant decrease in conductivity as film thickness decreases, in particular for films below 50 nm. Thicker films (160 nm) present an increase in conductivity of approximately a factor of 2 at high humidity levels (RH of 85%) when compared to films of 10 nm or lower. A more drastic effect is observed at lower humidity levels, where the difference in conductivity can reach a factor of 10−20. Similar effects of conductivity with thickness have been reported previously, although for thicknesses greater than the ones reported in this work. The previous results also showed less drastic effects due to confinement likely due to sample preparation differences including film deposition method, solvent, and drying procedures.[10] There are virtually no reports of the conductivity of films below 10 nm, and it is in this thickness regime where stronger ionic-transport limitations are observed. It is pertinent to mention that the self-assembled films with nominal thicknesses of less than 50 nm exhibit hydrophilic surfaces whereas the thicker films exhibit hydrophobic behavior.[40] Comparing the surface energies of the top interface of the thin films suggests that these films have similar nanostructures but that they differ from those exhibited by the thicker films as indicated by the abrupt change in surface energy.

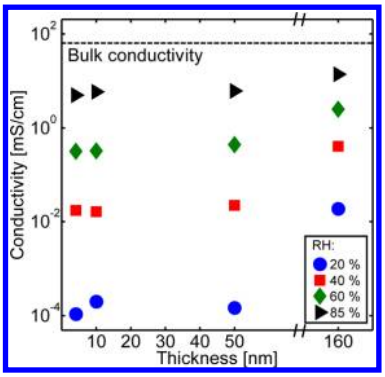

Figure 2. Conductivity of thin films as a function of hydrated film thickness and relative humidity (RH) including the value for a bulk Nafion 117 membrane under water−vapor-equilibrated conditions (dotted line).[47] Thinner films show decreased ionic conductivity, in particular at low humidity.

Water Uptake and Swelling. To elucidate the nature of the ionic-transport suppression of Nafion thin films, the water uptake was assessed both by measuring the thickness swelling and the mass uptake at various humidity levels. Figure 3 presents both the changes in thickness and hydration number (λ) as a function of RH and initial (dry) film thickness. Film swelling drastically increases as the initial thickness decreases for films deposited on thermal oxide SiO_2 surfaces. This result is in contrast with previous measurements of drop-cast films on Au QCM substrates where lower water uptake was observed for films of decreasing thickness.[48] It has been previously reported that wetting interactions at the film/substrate interface can affect the ionomer morphology and water uptake, which can explain the water-sorption discrepancies between films cast on

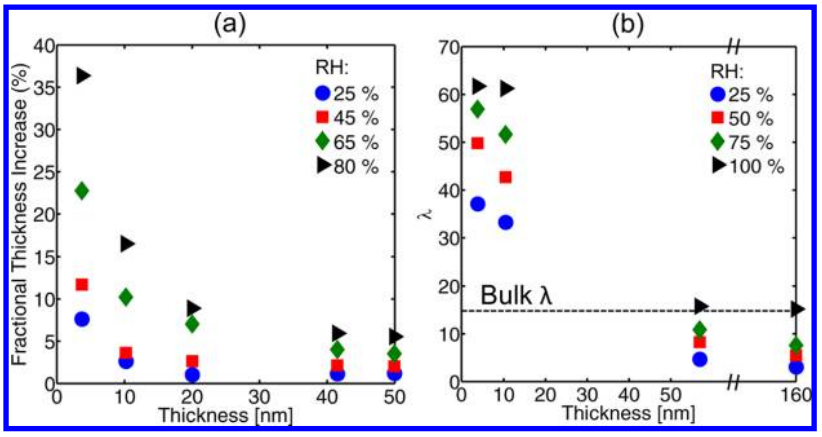

Figure 3. Thickness changes upon water uptake (left) and λ values (mol of H_2O/mol of sulfonic acid group) (right) show that thinner films uptake significantly more water than thicker and even saturated-vapor-equilibrated bulk Nafion 117 (dotted line) at all humidity levels.

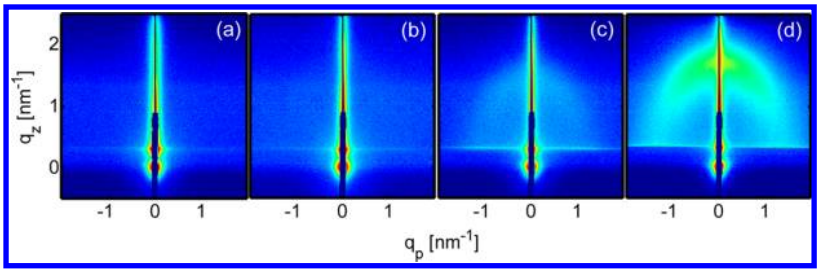

Figure 4. 2D GISAXS patterns from Nafion films of (a) 4, (b) 10, (c) 50, and (d) 160 nm in thickness equilibrated at 100% RH. The patterns presented only show scattering arising from periodic ionic domains for films of 50 and 160 nm in thickness. Thinner films do not show any appreciable scattering, suggesting a loss in correlations between ionic domains in the polymer (q_p refers to the in-plane scattering vector, and q_z corresponds to the out-of-plane scattering vector).

different substrates.[33] To support the swelling results from ellipsometry, QCM measurements were used to measure the total amount of water sorbed into the Nafion thin-film samples. This measurement is different than most QCM measurements on thin polymer films in the literature as we employed QCM crystals that were sputtered with SiO_2 on top of the Au electrode to form a surface that resembles the thermally grown SiO_2 surface in the ellipsometry experiments. The sputtered SiO_2 QCM crystals did not have any measurable water uptake as a function of RH for the bare crystals. The data in Figure 3 show that the thinner films, 4 and 10 nm, absorbed significantly more water on a relative basis than the thicker 57 and 160 nm films (see Supporting Information for mass uptake data). The hydration values for the thicker films are in the range observed for Nafion membranes under these conditions.[33] The hydration numbers and corresponding mass uptakes of the 4 and 10 nm samples were very high, which is a result of the effect of the surface composition on the thin-film properties.

It is important to point out that the trends in thickness swelling from ellipsometric measurements were more systematic than what was observed in the QCM water-uptake experiments. The thin-film samples had to be fabricated on the QCM crystals while the crystals were sealed in the crystal holder. This procedure resulted in some nonuniformities and edge effects in the film preparation on QCM crystals while films adsorbed on Si wafers with thermal oxide were perfectly smooth. Hence, the samples for QCM and ellipsometry were not exactly equivalent due to the preparation method differences. Nevertheless, the ellipsometry and QCM measurements reveal that Nafion thin films on SiO_2 surfaces swell much differently than Nafion thin films on Au surfaces[48] and perhaps in fuel-cell catalyst layers, which also exhibit lower water contents than the bulk membrane.[49] The findings herein are also significant for contacts with photovoltaic components and in fuel cells where oxide supports are beginning to be used in catalyst layers in place of the more traditional carbon or metal blacks. These results also underscore the importance of the substrate wetting interactions on influencing Nafion thin-film properties.

Morphology. As described above, both conductivity and water uptake are significantly affected by ionomer confinement in the thin films. Morphological characteristics of the material can be affected by confinement and in turn result in changes in the transport characteristics. To understand how the morphology of confined Nafion films affects transport, GISAXS patterns were obtained for films of different thicknesses after equilibration in a vapor-saturated environment (Figure 4). Patterns from thicker films (50 and 160 nm) show typical scattering characteristics due to correlations among ionic domains (intensity peak 1−2 nm^{-1}), as observed previously in the literature for Nafion films.[18,33,35] Additionally, anisotropy in the intensity distribution of the ionomer ring arises due to in-plane confinement effects. Because of this effect, film swelling in the in-plane direction is limited, whereas that in the direction normal to the substrate is unconfined; this results in greater levels of uptake from domains with periodicity in the out-of-plane direction as evidenced by higher ionomer scattering intensity in the GISAXS patterns away from the specular position. This effect is more pronounced for films cast from solution as polymer bundles tend to align parallel to the substrate.[18,35] Interestingly, for thinner films (4 and 10 nm) these characteristics disappear, and the scattering pattern only

dx.doi.org/10.1021/ma301999a | *Macromolecules* 2013, 46, 867−873

shows the specular reflection from the substrate and an intensity decay suggesting a lack of correlations in the film structure. The line profiles at the specular position clearly show the difference in scattering for these four films (Figure 5). They

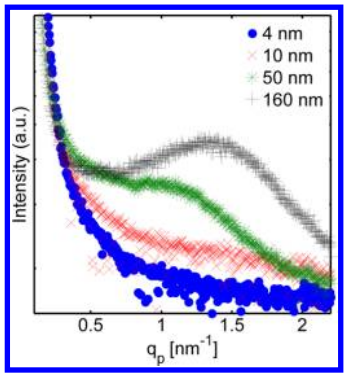

Figure 5. Line cuts from the GISAXS patterns for q_p at the specular position only show an intensity decay for 4 and 10 nm films and no indication of order in the films, while 50 and 160 nm films present a typical ionomer peak resulting from correlations between conducting domains.

also indicate that for films of 50 nm in thickness the domain size (d-spacing = 5.7 nm) is larger than for the thicker 160 nm films (d-spacing = 4.5 nm), which is consistent with a higher degree of water uptake as described earlier.

To complement the GISAXS results, TEM of films of various thicknesses was performed. It is important to point out that since the TEM images were obtained under a high-vacuum environment and used slightly different casting techniques, the structures observed are expected to differ quantitatively from those inferred from the X-ray scattering results collected for the hydrated films. Nevertheless, the structural information provided by the TEM measurements of the dry films can facilitate a qualitative understanding of the behavior of the material as a function of sample thickness. In Figure 6a–c, bright-field TEM images of 100, 20, and 10 nm Nafion thin films, respectively, are presented. Microphase separation in the thin films is evidenced by the dark and light contrast observed. As the films become thinner, the difference in contrast is reduced, suggesting an increase in domain mixing, i.e., a decrease in the degree of phase separation. The corresponding chemical maps for these films, obtained by low-loss spectrum imaging, are shown in Figure 6d–f. Red and green color coding is used to show the spatial distributions of two distinct chemical phases detected (see Supporting Information). The chemical maps underscore the decrease in phase separation already observed in bright-field mode for decreasing film thickness, correlating well with the GISAXS results.

DISCUSSION

The above data are consistent with Nafion films losing their internal conductive pathways as their thickness decreases below 50 nm. The morphological characteristics inferred from the X-ray scattering results suggest that as films are confined to thicknesses of a few nanometers, significant limitations for self-assembly arise and restrict the material from microphase separating into periodic ionic domains such as the ones observed in bulk Nafion membranes. This restriction can result in a higher degree of phase mixing in the material which can affect the structural integrity of the hydrophobic phase and so allow for the observed higher levels of water uptake. This result is not surprising since the chemical dissolution energies overcome the mechanical support energies in very thin films probably due to a lack of large backbone bundles with strong interchain interactions and due to low crystallinity;[19,24,33] in the bulk, the crystalline domains have a characteristic size of 15–20 nm, yet when films are confined to thicknesses below this range the formation of crystallites or large bundles of interacting chains is limited. This lack of mechanical rigidity results in a more homogeneous structure and the unusually high levels of swelling for thinner films (less than 10 nm). Similarly, the very thin films might also be limited in their ability to attain a high-conductivity morphology due to surface interactions and thickness of the films that result in a more hindered bundled lamellar structure. It is worth noting that the results discussed in this study correspond to films generated from Nafion

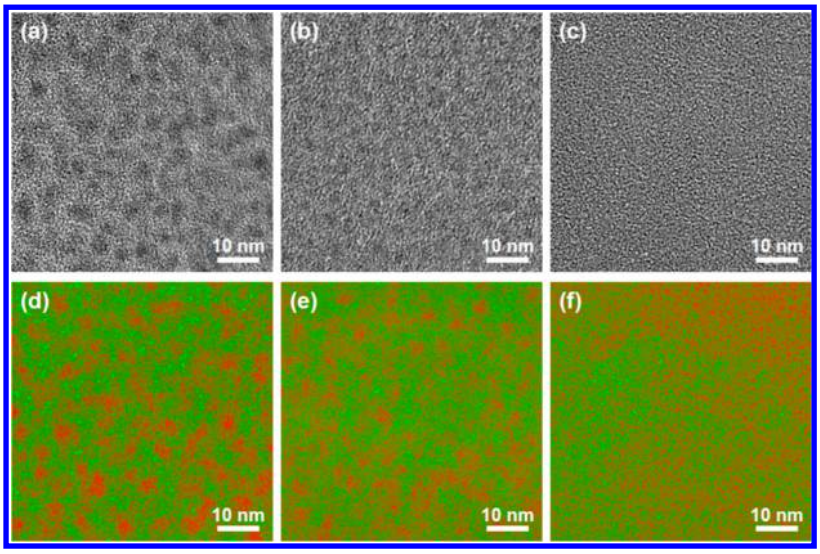

Figure 6. Bright-field TEM images (a–c) of 100, 20, and 10 nm films, respectively, show a reduction in contrast between the two phases as the film thickness decreases. Chemical maps obtained for the same set of films are presented in (d–f). A decrease in the degree of phase separation for decreasing film thickness is observed.

dx.doi.org/10.1021/ma301999a | *Macromolecules* 2013, 46, 867–873

solutions in IPA/water mixtures using self-assembly methods described in the literature.[11,40] Unlike drop-casting and spin-coating methods, the films are formed during the immersion of substrate over an extended period of time in the Nafion solution of fixed composition. Some rearrangement of the structure is expected when the substrate is withdrawn from the solution and evaporation of the solvent takes place. These solvent and processing effects are important in the case of Nafion, as it tends to form kinetically trapped morphologies that may show different structural and transport characteristics.[34] It is important to note that films analyzed in this work were deposited from solutions of different solvent compositions, and this in turn can have effects in the ultimate nanostructure of the material. To analyze the extent of these solvent effects, the morphology of thin films cast from solutions diluted with water (as opposed to IPA) was assessed using GISAXS and TEM (Figure S5). The obtained results demonstrate that these films also show a loss of microphase separation when confined to less than 10 nm of thickness and suggest that solvent composition differences are not significant in the self-assembly behavior of very thin films.

Although Nafion conductivity for bulk membranes has been shown to increase with membrane water content, the conductivity behavior of thin films is likely to differ significantly. Thinner films uptake more than 5 times the amount of water compared to bulk Nafion, and this large water sorption can result in dilution and isolation of the sulfonic acid groups within the sample and decrease the conductivity of the material. Also, a water layer can form at the interface between the polymer film and the substrate as a result of this uptake. This is particularly expected for films cast on SiO_2 substrates, as they delaminate upon immersion in liquid water. The presence of an interfacial layer of water will certainly result in more pronounced effects on both the water uptake and conductivity of thinner films, as this layer would make up a larger volume fraction of the films; however, the observed high water contents suggest that any water film is essentially still solvating the ionic groups and a definable structure of separate water and polymer becomes more ill-defined. In addition, at moderate humidities, while the water sorption is high, the conductivity remains low probably due to the surface interactions and the morphology.

It is notable that the thicker films approach the canonical relationship and values for bulk Nafion conductivity, while the thin films demonstrate a significant deviation. One does not expect such a large deviation as the GISAXS results imply a more continuous morphological change, and more data are required to define the relationship accurately. However, in support of the above picture of ionic group dilution, the data for the ionic conductivity of Nafion at very high water contents ($\lambda \sim 60$) is consistent with that of Gebel where he measured conductivity of hyperswollen Nafion membranes.[50] As a final note, if Nafion thin films adopt a lamellar structure for decreasing thickness, then one might expect the conductivity to become more anisotropic and perhaps even increase as film thickness decreases. This effect would be also consistent with some entropic arguments where the clustering decreases with thickness and the increased mixing will help conduction.[51] The lack of such a correlation suggests that the loss of domain structure and dilution of ionomer domains at increased levels of water uptake dominates the behavior of the adsorbed thin films in this study.

CONCLUSIONS

This work demonstrates that thin-film confinement can strongly affect both the structure and properties of Nafion. When Nafion films are confined to thicknesses below 10 nm, a drastic change in the microstructure of the material is observed. In this thickness regime, significant limitations to self-assembly exist which result in a lower degree of phase separation between the ionic domains and the matrix as demonstrated both by GISAXS and TEM measurements. The lack of structural integrity of the thinner films as well as their higher surface to volume ratio allow for a higher degree of swelling of the material as observed from water-uptake measurements, resulting in large λ values of up to 60 molecules of water per sulfonic acid group. Consequently, the conductivity of thin films is also affected by confinement. Thinner films show a decrease in conductivity caused by the lower degree of phase separation between conducting and structural domains, as well as an expected isolation of sulfonic-acid groups by the large amount of water absorbed by the material. As films increase in thickness, their morphology shows a higher degree of phase separation, an increase in the order of conducting domains, a decrease in the amount of water uptake, and ultimately conductivity values that approach those of bulk Nafion. The confinement effects observed here together with wetting interactions effects reported elsewhere[18,33,35,36] can provided insights into the ion- and water-transport behavior in fuel-cell catalyst layers as well as other electrochemical devices including solar-fuels generators operating under humidified vapor conditions.

ASSOCIATED CONTENT

Supporting Information

Substrate preparation procedures, sample impedance spectra, ionic conductivity data, QCM mass-uptake data, TEM chemical maps, and characterization of films cast from water diluted solutions. This material is available free of charge via the Internet at http://pubs.acs.org.

AUTHOR INFORMATION

Corresponding Author

*E-mail mams@berkeley.edu.

Present Address

[#]Department of Chemical & Petroleum Engineering, The University of Calgary, Calgary, Alberta, Canada T2N 1N4.

Author Contributions

The manuscript was written through contributions from all authors. All authors have given approval to the final version of the manuscript.

Notes

The authors declare no competing financial interest.

ACKNOWLEDGMENTS

This material is based upon work performed by the Joint Center for Artificial Photosynthesis, a DOE Energy Innovation Hub, as follows: Characterization work performed by M.A.M. and R.A.S. was supported through the Office of Science of the U.S. Department of Energy under Award DE-SC0004993. Characterization work of F.I.A. and data analysis and project framing by A.Z.W. were supported by the Assistant Secretary for Energy Efficiency and Renewable Energy, Fuel Cell Technologies Program, of the U.S. Department of Energy under Contract DE-AC02-05CH11231; the researchers from

Penn State acknowledge the support of the U.S. Department of Energy, the Office of Energy Efficiency and Renewable Energy, the Fuel Cells Technology Program through a subcontract from General Motors Corporation under Grant DE-EE0000470; the researchers from Queen's University acknowledge financial support from Natural Sciences and Engineering Research Council of Canada (NSERC). We thank Dr. Alex Hexemer, Dr. Eric Schaible, Eun Lim, and Steven A. Alvarez for helpful discussions and facilitating the use of equipment at ALS. We also gratefully acknowledge Dr. Ahmet Kusoglu and Dr. Guillaume Sudre for helpful discussions. This work made use of facilities at the Advanced Light Source (ALS) and the National Center for Electron Microscopy (NCEM), both supported by the Office of Science, Office of Basic Energy Sciences, of the U.S. Department of Energy (Contract DE-AC02-05CH11231).

REFERENCES

(1) Weber, A. Z.; Mench, M. M.; Meyers, J. P.; Ross, P. N.; Gostick, J. T.; Liu, Q. H. *J. Appl. Electrochem.* **2011**, *41* (10), 1137−1164.
(2) Dresselhaus, M. S.; Crabtree, G. W.; Buchanan, M. V. *MRS Bull.* **2005**, *30* (7), 518−524.
(3) Inzelt, G.; Pineri, M.; Schultze, J. W.; Vorotyntsev, M. A. *Electrochim. Acta* **2000**, *45* (15−16), 2403−2421.
(4) Macknight, W. J.; Earnest, T. R. *J. Polym. Sci., Part D: Macromol. Rev.* **1981**, *16*, 41−122.
(5) Spurgeon, J. M.; Walter, M. G.; Zhou, J. F.; Kohl, P. A.; Lewis, N. S. *Energy Environ. Sci.* **2011**, *4* (5), 1772−1780.
(6) Spurgeon, J. M.; Lewis, N. S. *Energy Environ. Sci.* **2011**, *4* (8), 2993−2998.
(7) Makharia, R.; Mathias, M. F.; Baker, D. R. *J. Electrochem. Soc.* **2005**, *152* (5), A970−A977.
(8) Mashio, T.; Malek, K.; Eikerling, M.; Ohma, A.; Kanesaka, H.; Shinohara, K. *J. Phys. Chem. C* **2010**, *114* (32), 13739−13745.
(9) Xie, Z.; Navessin, T.; Shi, K.; Chow, R.; Wang, Q.; Song, D.; Andreaus, B.; Eikerling, M.; Liu, Z.; Holdcroft, S. *J. Electrochem. Soc.* **2005**, *152* (6), A1171−A1179.
(10) Siroma, Z.; Ioroi, T.; Fujiwara, N.; Yasuda, K. *Electrochem. Commun.* **2002**, *4* (2), 143−145.
(11) Paul, D. K.; Fraser, A.; Pearce, J.; Karan, K. *ECS Trans.* **2011**, *41* (1), 1393−1406.
(12) Mauritz, K. A.; Moore, R. B. *Chem. Rev.* **2004**, *104* (10), 4535−85.
(13) Gierke, T. D.; Munn, G. E.; Wilson, F. C. *J. Polym. Sci., Polym. Phys. Ed.* **1981**, *19* (11), 1687−1704.
(14) Gebel, G. *Polymer* **2000**, *41* (15), 5829−5838.
(15) Kim, M. H.; Glinka, C. J.; Grot, S. A.; Grot, W. G. *Macromolecules* **2006**, *39* (14), 4775−4787.
(16) Schmidt-Rohr, K.; Chen, Q. *Nat. Mater.* **2008**, *7* (1), 75−83.
(17) Rubatat, L.; Rollet, A. L.; Gebel, G.; Diat, O. *Macromolecules* **2002**, *35* (10), 4050−4055.
(18) Bass, M.; Berman, A.; Singh, A.; Konovalov, O.; Freger, V. *Macromolecules* **2011**, *44* (8), 2893−2899.
(19) Kusoglu, A.; Savagatrup, S.; Clark, K. T.; Weber, A. Z. *Macromolecules* **2012**, *45*, 7467−7476.
(20) Mauritz, K. A.; Moore, R. B. *Chem. Rev.* **2004**, *104* (10), 4535−4585.
(21) Onishi, L. M.; Prausnitz, J. M.; Newman, J. *J. Phys. Chem. B* **2007**, *111* (34), 10166−10173.
(22) Zawodzinski, T. A.; Derouin, C.; Radzinski, S.; Sherman, R. J.; Smith, V. T.; Springer, T. E.; Gottesfeld, S. *J. Electrochem. Soc.* **1993**, *140* (4), 1041−1047.
(23) Onishi, L. Equilibrium and transport properties of a proton-exchange membrane for fuel cells. University of California, Berkeley, CA, 2009.
(24) Kusoglu, A.; Modestino, M. A.; Hexemer, A.; Segalman, R. A.; Weber, A. Z. *ACS Macro Lett.* **2012**, *1* (1), 33−36.
(25) Weber, A. Z.; Newman, J. *J. Electrochem. Soc.* **2004**, *151* (2), 311−325.
(26) Eikerling, M.; Kornyshev, A. A.; Kucernak, A. R. *Phys. Today* **2006**, *59* (10), 38−44.
(27) Albert, J. N. L.; Epps Iii, T. H. *Mater. Today* **2010**, *13* (6), 24−33.
(28) Segalman, R. A. *Mater. Sci. Eng., R* **2005**, *48* (6), 191−226.
(29) Fasolka, M. J.; Mayes, A. M. *Annu. Rev. Mater. Res.* **2001**, *31* (1), 323−355.
(30) Russell, T. P.; Lambooy, P.; Kellogg, G. J.; Mayes, A. M. *Physica B: Condens. Matter* **1995**, *213-214* (0), 22−25.
(31) Huang, E.; Russell, T. P.; Harrison, C.; Chaikin, P. M.; Register, R. A.; Hawker, C. J.; Mays, J. *Macromolecules* **1998**, *31* (22), 7641−7650.
(32) Mansky, P.; Russell, T. P.; Hawker, C. J.; Pitsikalis, M.; Mays, J. *Macromolecules* **1997**, *30* (22), 6810−6813.
(33) Modestino, M. A.; Kusoglu, A.; Hexemer, A.; Weber, A. Z.; Segalman, R. A. *Macromolecules* **2012**, *45* (11), 4681−4688.
(34) Eastman, S. A.; Kim, S.; Page, K. A.; Rowe, B. W.; Kang, S.; Soles, C. L.; Yager, K. G. *Macromolecules* **2012**, *45*, 7920−7930.
(35) Bass, M.; Berman, A.; Singh, A.; Konovalov, O.; Freger, V. *J. Phys. Chem. B* **2010**, *114* (11), 3784−3790.
(36) Freger, V. *J. Phys. Chem. B* **2008**, *113* (1), 24−36.
(37) Dishari, S. K.; Hickner, M. A. *ACS Macro Lett.* **2012**, *1* (2), 291−295.
(38) Paul, D. K.; Fraser, A.; Karan, K. *Electrochem. Commun.* **2012**, *13* (8), 774−777.
(39) Siroma, Z.; Kakitsubo, R.; Fujiwara, N.; Ioroi, T.; Yamazaki, S. I.; Yasuda, K. *J. Power Sources* **2009**, *189* (2), 994−998.
(40) Paul, D. K.; Karan, K.; Docoslis, A.; Giori, J. B.; Pearce, J. Submitted to *Macromolecules*.
(41) Hexemer, A.; Bras, W.; Glossinger, J.; Schaible, E.; Gann, E.; Kirian, R.; MacDowell, A.; Church, M.; Rude, B.; Padmore, H. *J. Phys.: Conf. Ser.* **2010**, *247*, 012007.
(42) Watanabe, M.; Allen, F. I. *Ultramicroscopy* **2012**, *113* (0), 106−119.
(43) Allen, F. I.; Watanabe, M.; Lee, Z.; Balsara, N. P.; Minor, A. M. *Ultramicroscopy* **2011**, *111* (3), 239−244.
(44) Loppinet, B.; Gebel, G. r. *Langmuir* **1998**, *14* (8), 1977−1983.
(45) Schlick, S.; Gebel, G.; Pineri, M.; Volino, F. *Macromolecules* **1991**, *24* (12), 3517−3521.
(46) Loppinet, B.; Gebel, G. r.; Williams, C. E. *J. Phys. Chem. B* **1997**, *101* (10), 1884−1892.
(47) Slade, S.; Campbell, S. A.; Ralph, T. R.; Walsh, F. C. *J. Electrochem. Soc.* **2002**, *149* (12), A1556−A1564.
(48) Kongkanand, A. *J. Phys. Chem. C* **2011**, *115* (22), 11318−11325.
(49) Kusoglu, A.; Kwong, A.; Clark, K. T.; Gunterman, H. P.; Weber, A. Z. *J. Electrochem. Soc.* **2012**, *159*, F530−F535.
(50) He, Q.; Kusoglu, A.; Lucas, I. T.; Clark, K.; Weber, A. Z.; Kostecki, R. *J. Phys. Chem. B* **2011**, *115* (40), 11650−7.
(51) Park, M. J.; Nedoma, A. J.; Geissler, P. L.; Balsara, N. P.; Jackson, A.; Cookson, D. *Macromolecules* **2008**, *41*, 2271−2277.